Asia-Pacific Journal of Atmospheric Sciences (2025) 61:4
https://doi.org/10.1007/s13143-024-00388-y

Online ISSN 1976-7951
Print ISSN 1976-7633

REVIEW

Comparative Analysis of GloSea6 Hindcasts for Two Extreme El Niño Events and Their Impact on Indo-Western North Pacific Climate

Seung-Hwon Hyun[1] · Seung-On Hwang[2] · Chao Liu[3] · Soon-Il An[3] · Yu-Kyung Hyun[2]

Received: 4 June 2024 / Revised: 19 December 2024 / Accepted: 20 December 2024 / Published online: 7 January 2025
© The Author(s) 2024

Abstract
In this study, GloSea6 hindcast (HCST) from the UK Met Office is used to investigate the model prediction skill for the impacts on the East Asian summer associated with two extreme El Niño cases (1997/1998 and 2015/2016). For the 1998 case, we found that GloSea6 model is able to predict the ocean–atmosphere circulations one to two seasons ahead, including the anomalously positive sea surface temperature (SST) in the Tropical Indian Ocean (TIO) and the anomalous anticyclone (AAC) in the Western North Pacific during the spring and summer seasons. However, for the 2016 case it fails to capture the observed fast cooling of the spring TIO SST and the rapid decaying of the summer AAC, due to an overestimated linkage between the summer TIO and the precedent winter El Niño. Physically, the exaggerated model SST warming over both the eastern and western Indian Ocean suppresses the development of the surface westerly wind that enhances the summer monsoon flow in the TIO and cools the warmed SST as in the real world. According to further analysis, the sensitivity of the TIO is linked to the formation of the spring AAC, which is influenced by the longitudinal position of warm Pacific SST, causing the HCST to display a more idealized El Niño-TIO-AAC teleconnection than the observations. Thus, simulating the decaying El Niño and its teleconnection to the TIO is crucial for reliable seasonal forecasts of East Asian climate during post-El Niño summers.

Keywords Extreme El Niño · El Niño teleconnection · Seasonal forecast · Asian summer monsoon

1 Introduction

The remote teleconnections of the El Niño Southern Oscillation (ENSO) to East Asia during the subsequent summer have been widely discussed in various studies (e.g. Wang et al. 2000; Lee et al. 2005; Xie et al. 2009; Shao et al. 2018). El Niño events, in particular, have been shown to exert a greater influence on the East Asian summer climate in its decaying phase compared to La Niña events (Zhang et al. 2024). This is attributed to the asymmetry in ENSO intensity, where El Niño events typically exhibit a larger amplitude than La Niña events (Jin et al. 2003; An and Jin 2004; Capotondi et al. 2015). Especially, some extreme El Niño cases have caused catastrophic heavy rainfall over the East Asia in the following summer (Lau and Weng 2001; Chen et al. 2018).

Previous studies have widely investigated the influences of El Niño on the low-level anticyclone (AAC) in the subtropical Western North Pacific (WNP) region (e.g. Klein et al. 1999; Wang et al. 2000, 2003, 2017; Wen et al. 2015; Xie et al. 2009, 2016). Wang et al. (2000) suggested that the AAC is forced by the secondary circulation originating from the tropical central Pacific cooling during the decaying El Niño phase. On the other hand, Xie et al. (2009) proposed the Indo-Western Pacific Ocean Capacitor (IPOC) mechanism, in which the anomalously warm Indian Ocean SST caused by El Niño teleconnection (Sobel et al. 2001; Chiang and Sobel 2002; Xie et al. 2002; An 2004), can persist into summer and generate the eastward propagating atmospheric Kelvin wave. The associated low-level easterly wind anomalies lead to meridional divergence in the boundary

✉ Seung-Hwon Hyun
shhyun@kiost.ac.kr

[1] Ocean Circulation and Climate Research Department, Korea Institute of Ocean Science and Technology, Busan, South Korea

[2] Climate Research Division, National Institute of Meteorological Sciences, Jeju 63568, Korea

[3] Irreversible Climate Change Research Center, Advanced Science and Technology Center, Yonsei University, Seoul, South Korea

layer and favor the establishment of the AAC in the WNP region. Therefore, the AAC may be further intensified by the wind-evaporation-SST feedback and reinforce the initial warming of the Indian Ocean. However, the East Asian summer climate exhibits complexity and many El Niño events do not conform to the idealized teleconnection mechanisms. For instance, it is noteworthy that the East Asian summer rainfall could be also related to intraseasonal climate variability and mid-latitude atmospheric perturbations, which are generally uncorrelated with tropical SST (Lee et al. 2005; Yoon and Yeh 2010; Li et al. 2017; Hyun and Yeh 2020).

The teleconnection uncertainties are evident even in extreme El Niño events. For example, the 1997/1998 event displayed strong ideal mechanisms of the IPOC effect and the AAC in the inter-seasonal teleconnection between the decaying El Niño and the summer Indo-WNP climate (Lau and Weng 2001; Xie et al. 2016). This is primarily attributed to the exceptionally strong heat release from the tropics into the atmosphere during the 1997/1998 El Niño event, which is considered the fundamental cause of the enhanced remote teleconnection. However, the 2015/2016 El Niño serves as a reminder that we should not generalize cases like the 1997/1998 event. Despite being classified as an extreme El Niño event, the 2015/2016 event exhibited atmospheric teleconnections that significantly differed from those of the 1997/1998 event (Santoso et al. 2017). For example, the 2016 AAC was relatively weak and did not persist into the late summer. Previous studies suggested that intraseasonal oscillation may play a more important role than the ENSO-IPOC mode in exciting the AAC in 2016 (Wang et al. 2020a). They also argued the role of the summer Madden–Julian Oscillation (MJO) in the monthly AAC during the late summers of 1998 and 2016 (Shao et al. 2018; Wang et al. 2020b). The differences between the summers of 1998 and 2016 indicate that even for extreme El Niño events, the impact on AAC in the following year can vary each other, and in some cases, prediction models may produce forecasts that differ significantly from real world.

In this paper, we aim to evaluate the forecasting performance of the Global Seasonal Forecasting System version 6 (GloSea6) of the UK Met Office, which is officially operated for seasonal forecasting by Korean Meteorological Administration (KMA), in ENSO teleconnections in the western North Pacific. Since this model is used for operational forecasting on seasonal time scales by public agencies, it is crucial to evaluate its ability to simulate the interaction of ocean–atmosphere during the decaying El Niño periods and analyze the reason of possible biases. For our evaluation, we aim to conduct an analysis comparing observations with the hindcast data (referred to as the HCST), which was generated using GloSea6 to recreate past seasonal forecast fields from 1993 to 2016. Specifically, we focus on the decay phase of two extreme El Niño events, the 1997/1998 and 2015/2016 cases, compare their teleconnection differences, and explore the underlying physics. The analysis of only these two extreme events takes into account the fact that the HCST period begins in 1993. Section 2 introduces the data sets and methods used in this study. The analysis and results are presented in Sect. 3. Summary and discussions are given in Sect. 4.

2 Data and Method

GloSea6 is an updated version of GloSea5 (MacLachlan et al. 2015) and consists of the Global Coupled version 3.2 (GC 3.2), Global Atmosphere version 7.2 (GA 7.2), Global Land version 8.0 (GL 8.0), Global Ocean version 6.0 (GO 6.0), and Global Sea Ice version 8.1 (GSI 8.1). The HCST is the reconstructed forecast data for the past climate in the same way as the operating climate forecasting using GloSea6. It produces forecast products at most of a 6-month lead using 28 ensemble members, which is achieved by initializing 7 different ensemble members with different initial conditions on the 1st, 9th, 17th, and 25th of each month. In our study, we used hindcast products initialized in February 1993 ~ 2016, whose prediction extends to August and covers the boreal spring and summer of the decaying ENSO phase. The prediction uncertainty associated with the internal variability is measured by the ensemble spread across 28 ensemble members. In the case of the observational anomaly located outside the model spread, we assume such the HCST failure is due to the model bias rather than the internal variability.

For verification, we investigated the same period (1993 ~ 2016) of the observation data. The precipitation data is from the Global Precipitation Climatology Project (GPCP) (Adler et al. 2018). SST and the horizontal wind field at 850 hPa level are derived from the fifth generation of ECMWF Re-Analysis (ERA5) (Hersbach et al. 2020).

ENSO index is defined as Niño 3.4 area-averaged SST anomaly in December-January–February (D(0)JF(1)) season. The AAC index is defined by the 850 hPa anomalous zonal wind difference between the northern (25°N ~ 35°N, 115°E ~ 145°E) and southern (5°N ~ 15°N, 115°E ~ 145°E) boxes. The anomalies for both 1998 and 2016 cases were calculated as deviations from the 24-year mean. For GloSea6 HCST, the anomalies for the two El Niño cases were defined as the difference between the ensemble mean of the two cases and the 24-year ensemble mean.

3 Results

3.1 Characteristics of Two Extreme El Niños in the Observations and the HCST

We first compared the large-scale atmospheric and oceanic conditions, i.e., anomalous SST, precipitation, and the

850 hPa low-level wind fields, between the observations and GloSea6 HCST for two extreme El Niño cases (i.e., 1997/1998 and 2015/2016) in their decaying spring and summer seasons (Fig. 1). During the 1998 March–April-May (MAM) season, there are positive SST anomalies over the equatorial Indian Ocean (EIO) and the tropical central-eastern Pacific, accompanied by large positive precipitation anomalies (Fig. 1a). In the north equatorial part of the western Pacific, the AAC generates SST cooling, which then propagates westward as an atmospheric Rossby wave in response to reduced precipitation (Wang et al. 2000). In response to the strong warming of the eastern equatorial Pacific, the AAC extends into the southeastern EIO, causing local anomalous easterly winds. This generates an oceanic downwelling Rossby wave that propagates into the western Indian Ocean (Xie et al. 2002), warming the entire EIO until the following summer season. In the 1998 June-July–August (JJA) season, the positive SST anomaly on the equatorial and the northern TIO develops, accompanied by intensified anomalous easterly wind on the southern WNP region. Additionally, the strong cold SST in the central Pacific and the zonal SST gradient between the Indo-western Pacific and the central Pacific further enhance the anomalous easterly wind and low-level convergence towards the EIO. At the same time, the stronger AAC and the rainband in the East Asian region are observed (Fig. 1b). Thus, it is reasonable to

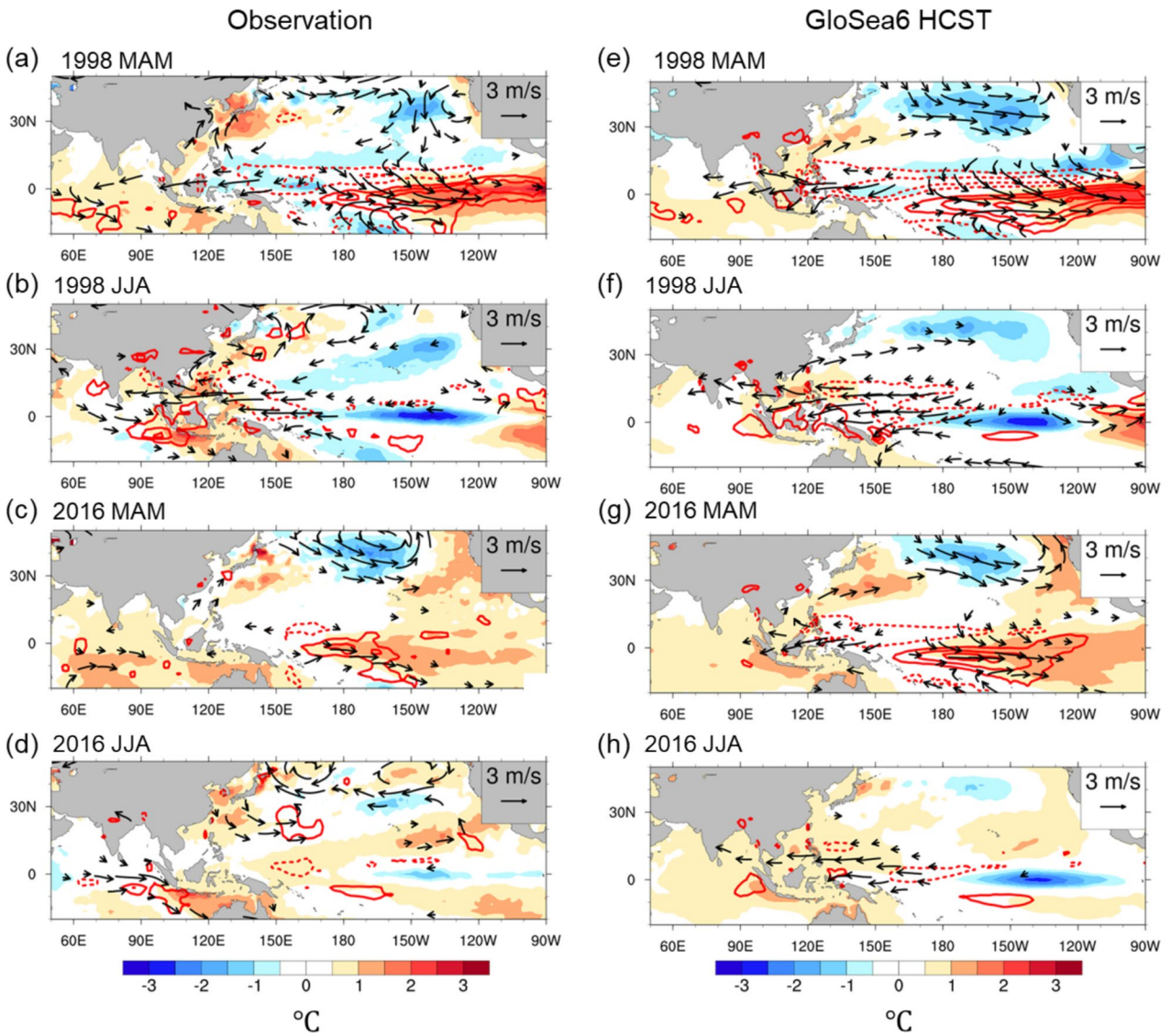


Fig. 1 Spatial distribution of SST (shading), 850 hPa wind (vectors), and precipitation (red contours) anomalies (**a**) in 1998 MAM, and (**b**) in 1998 JJA. For precipitation, the contour interval is 3 mm/day starting from 0 mm/day. (**c**) and (**d**) are the same as (**a**) and (**b**), but for 2016 MAM and JJA, respectively. (**e**)-(**h**) show the same as (**a**)-(**d**), but for 28 ensemble-averaged anomalies from 24 years-mean in GloSea6 HCST

hypothesize that this AAC is intensified by the IPOC effect through the eastward propagating convective Kelvin wave. This convective flow on Indian Ocean is also intensified by the colder SST of the central Pacific which makes a thermal contrast. Furthermore, due to the climatological northward shift of ICTZ to the summer hemisphere and the westward propagated atmospheric Rossby wave (Murakami and Matsumoto 1994; LinHo 2002), the AAC is maintained during the JJA season.

In the 2016 MAM (Fig. 1c), the anomalous positive SST and precipitation in the equatorial eastern Pacific (180˚W ~ 90˚W) are weaker than those in the 1998 MAM. Instead, spatial patterns of these two variables are more concentrated on the equatorial central Pacific (160˚E ~ 180˚E) than the 1998 MAM. In the Indo-western Pacific region, the oceanic and atmospheric responses over both the TIO and the WNP region are overall similar to the 1998 MAM, although the intensities of precipitation anomalies and the AAC flows are weaker. For the 2016 JJA, on the other hand, the positive SST anomalies on the western Indian Ocean become negative while the positive SST anomalies over the eastern and northern Indian Ocean are weakened, and the AAC is also not maintained like the 1998 summer (Fig. 1d). In particular, positive SST anomalies the central equatorial Pacific drive anomalous cyclonic circulation following the Gill-type response, which extends farther west into the western Pacific and weakens the formation of the AAC (Zhang et al. 2015; Jiang et al. 2019; Fan et al. 2023). The easterly winds on the southeastern EIO, typically driven by the extended AAC, are also not found. As the spring AAC does not form in the 2016 case due to the westward positive SST core (Fig. 1c), the warmed summer TIO SST is also less evident (Fig. 1c, d). This results in a faster decay of the positive SST anomaly over the Indian Ocean at the onset of the boreal summer, followed by the weaker SST than in the 1998 case. Consequently, the influence of 2015/2016 El Niño is weak in the Indian Ocean, and the IPOC effect is also weaker in the 2016 JJA than in 1998. Meanwhile, a positive rainfall anomaly developed at the far eastern part of the WNP region (150˚E ~ 180˚E) (Fig. 1d). Therefore, the teleconnection of El Niño-IPOC effect does not play a major role over the subtropical WNP region during the decaying period of 2015/2016 El Niño. In conclusion, these results confirmed that the temporal evolutions of 1997/1998 and 2015/2016 events are different from each other.

For the HCST results, both the MAM and JJA seasons of 1998 show spatial patterns that are broadly similar to the observations (Fig. 1e, f), despite some minor differences at the reginal level. In contrast, the longitudinal positioning of SST anomalies in the equatorial Pacific during the spring of 2016 shows differences between the HCST and the observations, unlike the 1998 (Fig. 1g). HCST shows an positive SST pattern in the Pacific that extends farther east during the MAM season of 2016. In the 2016 JJA season, the HCST displays anomalous warm SSTs across the entire tropical Indian Ocean (TIO) (Fig. 1h), whereas the observation shows an early negative Indian Ocean Dipole (IOD) pattern (Fig. 1d). Additionally, the HCST shows a meridional dipole pattern of precipitation associated with the WNP AAC, which is not found in the observation. These features of the 2016 HCST suggest that a more eastward-positioned MAM positive SST core in the model could be responsible for the extended maintenance of the AAC (Zhang et al. 2015; Jiang et al. 2019), and with a warmer TIO during JJA, compared to the observation.

For a detailed comparison between the HCST and the observations, we compute the spatial and seasonal differences (the HCST minus the observations) between their anomalies (Fig. 2). For the spring season of the 1998 case, the HCST shows a higher precipitation anomaly in the equatorial eastern Pacific and drier anomalies in the northern off-equatorial and the western equatorial Pacific than the observations (Fig. 2a). Furthermore, the colder SST in the TIO and the warmer SST in the western Pacific indicate that the influence of 97/98 El Niño is weaker in GloSea6 HCST than in the observations (Fig. 2e), despite their anomalous patterns are similar to each other (Fig. 1a, e). For the summer season of 1998, the HCST reveals much wetter anomalies over the maritime continents (the southern WNP region) compared to the observation (Fig. 2b), and this difference falls outside of the ensemble spread of the HCST at 95% confidence level. Additionally, the East Asian summer rainband appears at a further southern latitude (near Taiwan) in the HCST than in the observation. This modeling error originates from the difference in the spatial distribution and intensity of the AAC in GloSea6. The wetter eastern and drier western part of the WNP region indicates the more westward located AAC in the HCST. (Fig. 2f).

For the 2016 case, the significant differences between the HCST and the observations appear primarily in the central Pacific during the spring season (Fig. 2c, g). The HCST exhibits larger positive anomalous precipitations than the observations over the near-central and eastern equatorial Pacific during this time (Fig. 2c). Furthermore, the warmer (colder) anomalous SST in the equatorial eastern (central) Pacific region is found, suggesting that the 2016 case in the HCST is more similar to the 1998 case of a typical EP El Niño (Fig. 2g). In the TIO region, a slightly warmer SST appears from the early spring in the western EIO (WEIO), propagating eastward from the spring to the summer season. During the summer season of 2016, the HCST shows a statistically significant warmer SST on the entire TIO than the observation, causing a more positive precipitation in that region (Fig. 2d, h). This convective activity generates stronger westerly wind flow from the WP to the eastern EIO (EEIO) compared to the observation. The difference also

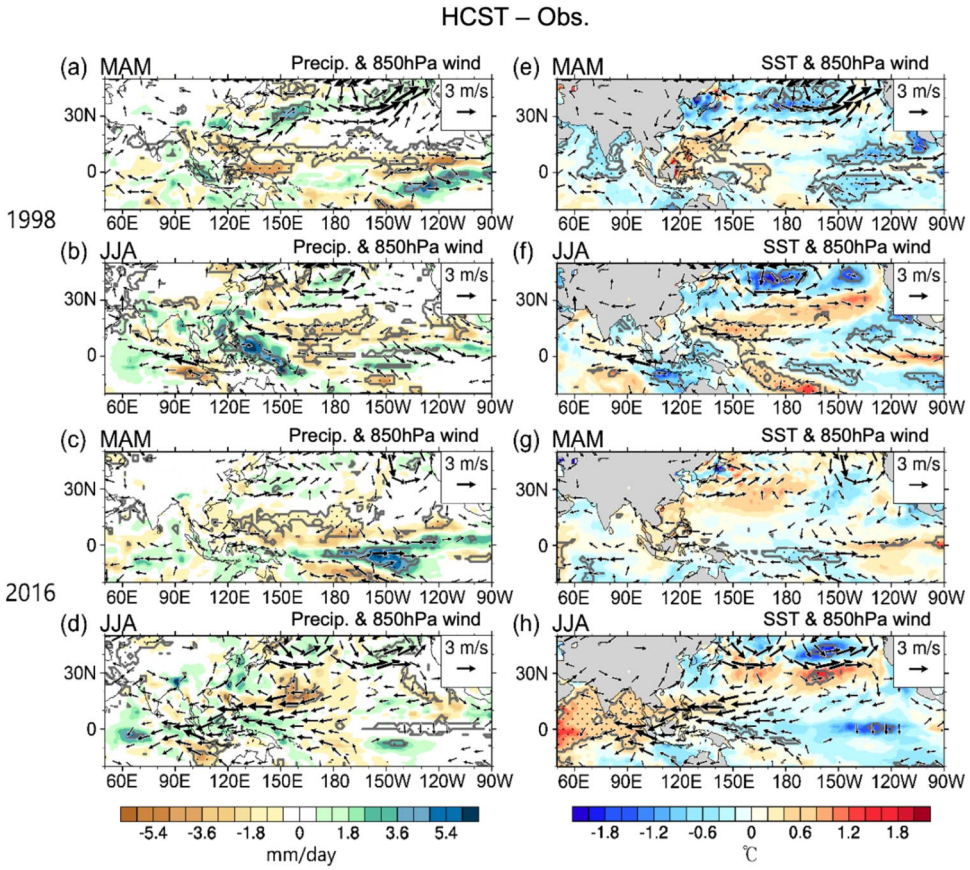


Fig. 2 Difference in anomalies between GloSea6 HCST and the observations (the HCST minus the reanalysis. The left column shows precipitation (color) and 850 hPa wind (vectors) for (**a**) (**b**) 1998, and (**c**)(**d**) 2016. The right column shows the same as the left column, except for SST (color) for (**e**)(**f**)1998, and (**g**) (**h**)2016. Stippled areas denote regions outside the ensemble spread of the HCST with the 95% probability

exhibits a more drought pattern in the subtropical WNP (10˚N ~ 30˚N) region as well as a more anticyclonic low-level wind field in the WNP than the observation (Fig. 2d). These statistically significant discrepancies with the observations support our claim that the exaggerated simulations of the IPOC effect in the 2016 HCST are the main cause for the overestimated AAC. Consequently, the biased sensitivity of the WEIO to the decaying El Niño and the biased climate of the TIO and the WNP regions in the 2016 summer are coupled to each other, suggesting fundamental discrepancies in GloSea6 model simulations. These results suggest that the primary discrepancies between the HCST and the observations in 2016 are most pronounced in the response of the equatorial Indian Ocean and western Pacific during the decaying El Niño phase. To identify which processes are hindering the simulation of the WEIO cooling in the 2016 HCST, it is necessary to conduct a more detailed analysis in a finer temporal scale beyond seasonal means.

To compare the equatorial processes between GloSea6 HCST and the observations, we present the Hovmöller diagram of the air-sea characteristics in the equatorial (10ºS ~ 10ºN) Indian-Western Pacific (Fig. 3). Comparing observations of two El Niño cases, the 1998 case exhibits a narrow coastal cooling SST in the WEIO that starts from July (Fig. 3a), while the 2016 case shows a fast and wide SST cooling pattern in the western and central EIO from May (Fig. 3b). In the 2016 case, however, the warmed WEIO SST is mostly absent except for a short period in spring, and the precipitation pattern displays a zonal dipole pattern with negative anomalies in the western Indian Ocean and positive anomalies in the EEIO. This indicates significant differences in the interbasin processes during the decaying periods of the two El Niño events. The warmed TIO in the observation begins to dissipate in late spring and early summer due to anomalous westerly winds in the EIO and atmospheric convective activity associated with the MJO, which causes a cooling of the western Indian Ocean and a negative IOD pattern (Lu et al. 2018). These cooling processes make the precipitation anomaly and the convective center move to the EEIO region during the summer season (Fig. 3a, b). For GloSea6 HCST (Fig. 3c), the 1998 case shows a similar late SST cooling pattern in the WEIO and the summer precipitation to the observations, although the anomalies are weaker. However, in the 2016 case, the WEIO cooling is not captured by the model (Fig. 3d), and the atmospheric convective center appears in the central EIO similar to the 1998 case. This warm IO, which is caused from the warm WEIO in the early spring, interrupts the sudden anomalous westerly winds as observed in May 2016 (Fig. 3f). Further

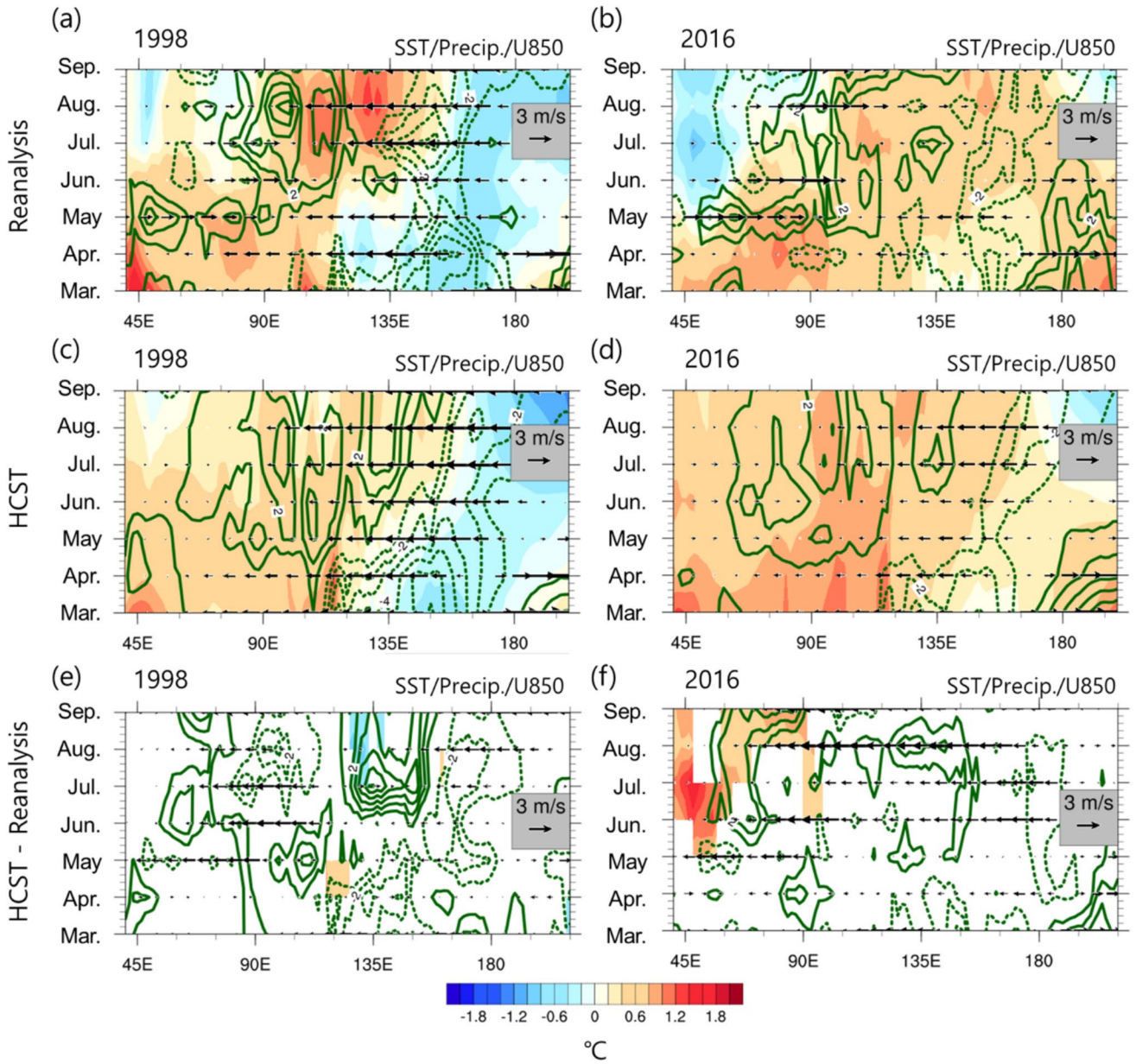


Fig. 3 Hovmöller diagrams of surface temperature, precipitation, and 850 hPa zonal wind in the equatorial Indo-Pacific Ocean (10˚S ~ 10˚N, 40˚E ~ 200˚E) during the decaying periods of two extreme El Niño events. (**a**),(**c**) and (**e**) for 1998, (**b**), (**d**) and (**f**) for 2016. The top panel shows the observation data, the middle panel shows GloSea6 HCST, and the bottom panel displays the differences (the HCST minus the observations). Colored areas in (**e**)(**f**) denote regions outside the ensemble spread of the HCST with the 95% probability

analysis reveals that differences in the summer EIO are closely linked to the longitudinal positioning of Pacific SST anomalies starting from March (Fig. S1), supporting the idea that the eastward positioning of positive SST from March 2016 in the HCST contributes to the maintenance of a warm TIO during summer, as discussed in Fig. 1 before. Consequently, the warmed TIO of the 2016 case derives the exaggerated simulations of the IPOC effect in GloSea6 HCST.

3.2 Assessment of the HCST Performance in the Decaying El Niño Periods

To investigate the characteristics of these prediction biases, it is essential to examine the general features of simulated relevant variables in the model and compare them to the observation data. We analyzed the scatter plots of the WEIO SST anomalies against Niño3.4 SST for the MAM season from 1993 to 2016 (Fig. 4). The results show that in the

HCST, both Niño3.4 SST and the WEIO SST anomalies during the MAM season exhibit comparable magnitudes to the observations (Fig. 4a), displaying statistically significant correlation coefficient (R = 0.68 in the observations, R = 0.70 in the HCST). Notably, during the extreme El Niño events, the 1998 HCST is closely aligned with the observation in the MAM season, indicating that GloSea6 provides accurate predictions for the 1998 cases. However, the observation shows a high WEIO SST anomaly (over + 1.0 ℃) only in 1998 at 28.6℃ of Niño3.4 SST, whereas in 2016, the observed WEIO SST anomaly is weaker (+ 0.52℃) compared to the 1998 case. In contrast, GloSea6 tends to simulate more sensitive interbasin teleconnections between the decaying El Niño and the WEIO during the spring season. The disparity in interbasin sensitivities is more evident during the boreal summer season than the spring season (Fig. 4b). The HCST reveals a significant correlation coefficient (R = 0.72) between the summer WEIO (10˚S ~ 10˚N, 45˚E ~ 60˚E) SST and the preceding winter Niño3.4 SST, indicating a dominant influence of decaying El Niño on the WEIO from spring to summer. However, in the case of the observations, no significant correlation is shown (R = −0.09), suggesting that GloSea6 overestimates the sensitivity of the summer WEIO SST to El Niño SST forcing. Especially in the extreme El Niño cases, the HCST displays large positive summer WEIO SST anomalies, while the observations show low WEIO SST anomalies, 0.18℃ in 1998 and −0.51℃ in 2016.

By examining the monthly correlation coefficients of the WEIO SST against the observed Niño3.4 SST in the DJF season from 1993 to 2016 (Fig. 5a), it was found that the differences in the background sensitivities between the HCST and the observations arise from the sustained significant influence of El Niño on the WEIO region. The HCST shows higher coefficients from March (R = 0.82) to June (R = 0.75), whereas the observations show an insignificant correlation after May (R = 0.41), which further decreases to negative correlations. In the observations, the interseasonal influence of decaying El Niño events tends to persist from boreal spring to early summer (i.e., June to July) in the EEIO region (10˚S ~ 10˚N, 75˚E ~ 100˚E) (blue bars in Fig. 5b). However, the HCST shows that both the WEIO and the EEIO (yellow bars in Fig. 5a, b) are statistically correlated with Niño 3.4 SST index, indicating that the responses to El Niño SST are positive across the entire TIO region in the HCST. Additionally, in the observations, the zonal thermal contrast across the Indian Ocean intensifies surface westerly wind anomalies in the TIO region (10˚S ~ 10˚N, 60˚E ~ 100˚E) during the late spring, and this westerly wind shows statistically significant correlations with Niño 3.4 SST in the previous DJF. This suggests that the anomalous low-level westerly wind plays an important role in the decaying of the warmed TIO SST (Fig. 5c). The anomalous westerly winds lead to SST cooling in the TIO, disrupting the IPOC effect due to weakened convective activity. However, in GloSea6 HCST, the relatively warm SST in the WEIO tends to persist until the following summer season (Fig. 5a), and suppresses the formation of anomalous westerly winds in the TIO region (Du et al. 2009). Consequently, it is considered that the warmer spring WEIO SST compared to the observations trigger the maintenance of the warmed TIO until the summer season, then generates the convective Kelvin wave due to the IPOC effect (Xie et al. 2009; 2016). Since the EEIO generally exhibits a positive correlation with SST through the summer in both the HCST and the observations, the positive correlation of the WEIO SST in the HCST suggests that the entire warmed TIO continues throughout the summer, simulating the overestimated IPOC effect.

To investigate the difference of sensitivity in the Indian Ocean compared to the observations, we analyzed the correlation coefficient map between the observed DJF Niño 3.4 SST and the HCST-minus-observations differences in the decaying periods (Fig. 6). Compared to the observations, GloSea6 tends to simulate colder SSTs in the central Pacific and warmer SSTs in the eastern Pacific during early spring season following the mature phase of El Niño (Fig. 6a). This implies that the formation of the AAC in GloSea6 HCST,

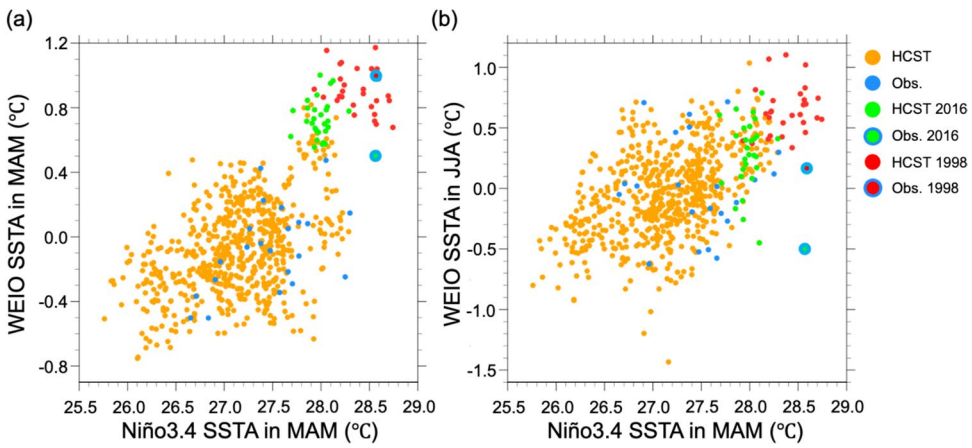


Fig. 4 Scatter plots of (**a**) MAM and (**b**) JJA seasonal mean SST anomalies in the WEIO (10˚S ~ 10˚N, 45˚E ~ 60˚E) against Niño3.4 during MAM for the years 1993–2016. Yellow dots represent GloSea6 HCST, red (green) dots represent the 1998 (2016) HCST, blue dots show the observations, and red (green) dots with blue outer lines correspond to the observations for 1998 (2016)

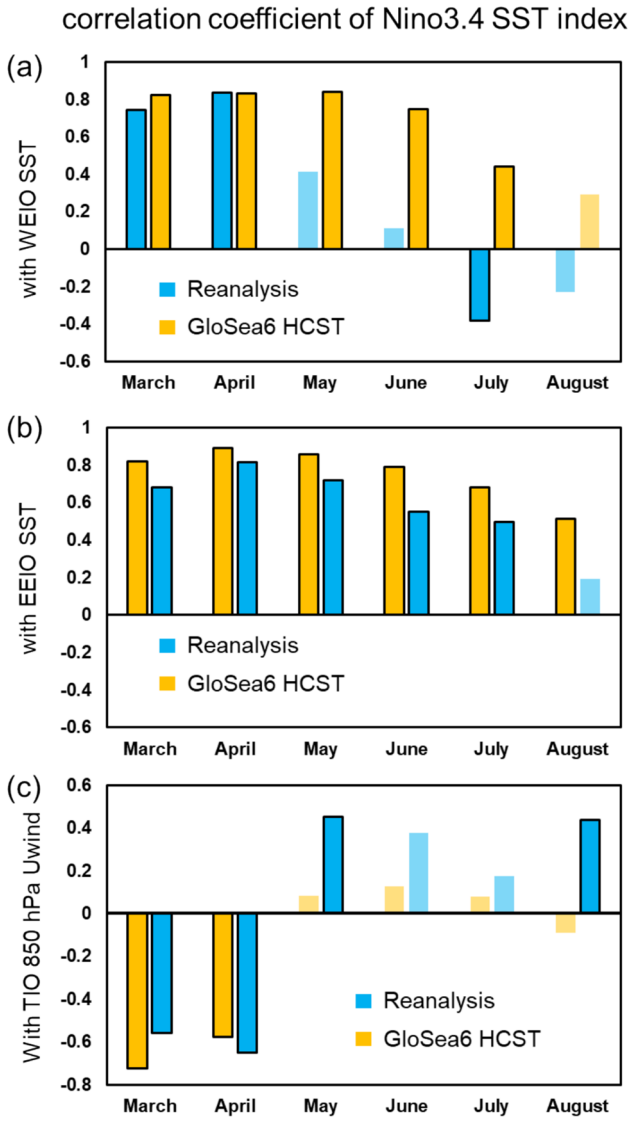


Fig. 5 Correlation coefficients between the observed Niño3.4 SST index (DJF season) and indices in the Indian Ocean during the months in the decaying El Niño period. (**a**) with the WEIO (10˚S ~ 10˚N, 45˚E ~ 60˚E) SST (**b**) with the EEIO (10˚S ~ 10˚N, 75˚E ~ 100˚E) SST and (**c**) with the TIO (10˚S ~ 10˚N, 60˚E ~ 100˚E) zonal wind in 850 hPa. Blue bars indicate reanalysis results, while yellow bars indicate GloSea6 HCST results. Bars with black lines show values that are significant at the 95% confidence level, while light-colored bars indicate values that are not significant

which shows colder spring SSTs in the central Pacific, occurs more easily compared to the observations (Zhan et al. 2015; Jiang et al. 2019). The stronger early spring AAC can induce an easterly wind anomaly over the Maritime Continent and the southeastern Indian Ocean during the late spring of decaying El Niño events (Fig. 6b). This anomalous easterly wind weakens the climatological westerly in the EIO, generating westward-propagating subsurface downwelling Rossby waves, which suppress the climatologically elevated thermocline in the WEIO (Xie et al. 2002). Through this process, the elevated SST in the WEIO disrupts the formation of anomalous westerly winds and prevents the overall SST cooling across the TIO, resulting in a higher summer SST in the TIO compared to the observations (Fig. 6c). The spatial pattern of correlation coefficient map shows similarity with the differences pattern between the HCST and the observations in the 2016 case (Fig. 2g, h and Fig. S1) which shows the colder (warmer) central (eastern) equatorial Pacific and the warmer WEIO from the spring to the summer season. This indicates that GloSea6 model's failure in the decaying period of 2015/2016 El Niño event can be explained by the basic spatial difference in the simulation of El Niño decaying.

To further illustrate this point, we compute the 21-year moving correlation between the DJF averaged normalized Niño3.4 SST index and the AAC index for 1979 ~ 2016 (1993 ~ 2016) of the observations (the HCST), but excluding the two extreme El Niño cases of 1982/1983, 1997/1998 (Fig. 7). The correlation coefficients show insignificant relationships in the observations, meaning that significant correlations are primarily driven by a few extreme El Niño events in the real world. Although the last window (1996 ~ 2016) contains the 2015/2016 extreme El Niño event, the correlation remains insignificant, suggesting that the observations do not exhibit a robust teleconnection between El Niño and the summer AAC except for the 1997/1998 case. Meanwhile, the HCST shows significant coefficients (0.57 ~ 0.66), indicating that the HCST fails to accurately simulate the teleconnection of the decaying El Niño due to the idealized and overestimated warming of the TIO basin and the IPOC effect. These significances are consistent across other window lengths (not shown). Consequently, the observations do not show the idealized linear correlation between other ENSO events and the TIO SST anomalies during the JJA season, as simulated by the HCST (Fig. S2a), suggesting that the HCST reveals a more linear relationship between other ENSO events and the AAC than the observations (Fig. S2b). The processes in the Indo-Western Pacific in 1998 are considered unusual in the real world, whereas GloSea6 tends to simulate other El Niño events in a similar way to 1998 in general, with the 2016 HCST event also fitting into this pattern.

In conclusion, GloSea6 tends to simulate the longitudinal positioning of the warmer SST farther east in the Pacific during the decaying El Niño periods, compared to the observations. This results in the overestimated sensitivity of the WEIO to high SSTs in the following spring after El Niño events. Since El Niño-decaying sensitivities of high SST in the WEIO during the spring season following an El Niño are stronger than in the observations, GloSea6 tends to overestimate seasonal persistence of the IPOC effects during the 2016 JJA, unlike the real world. This can be identified as the

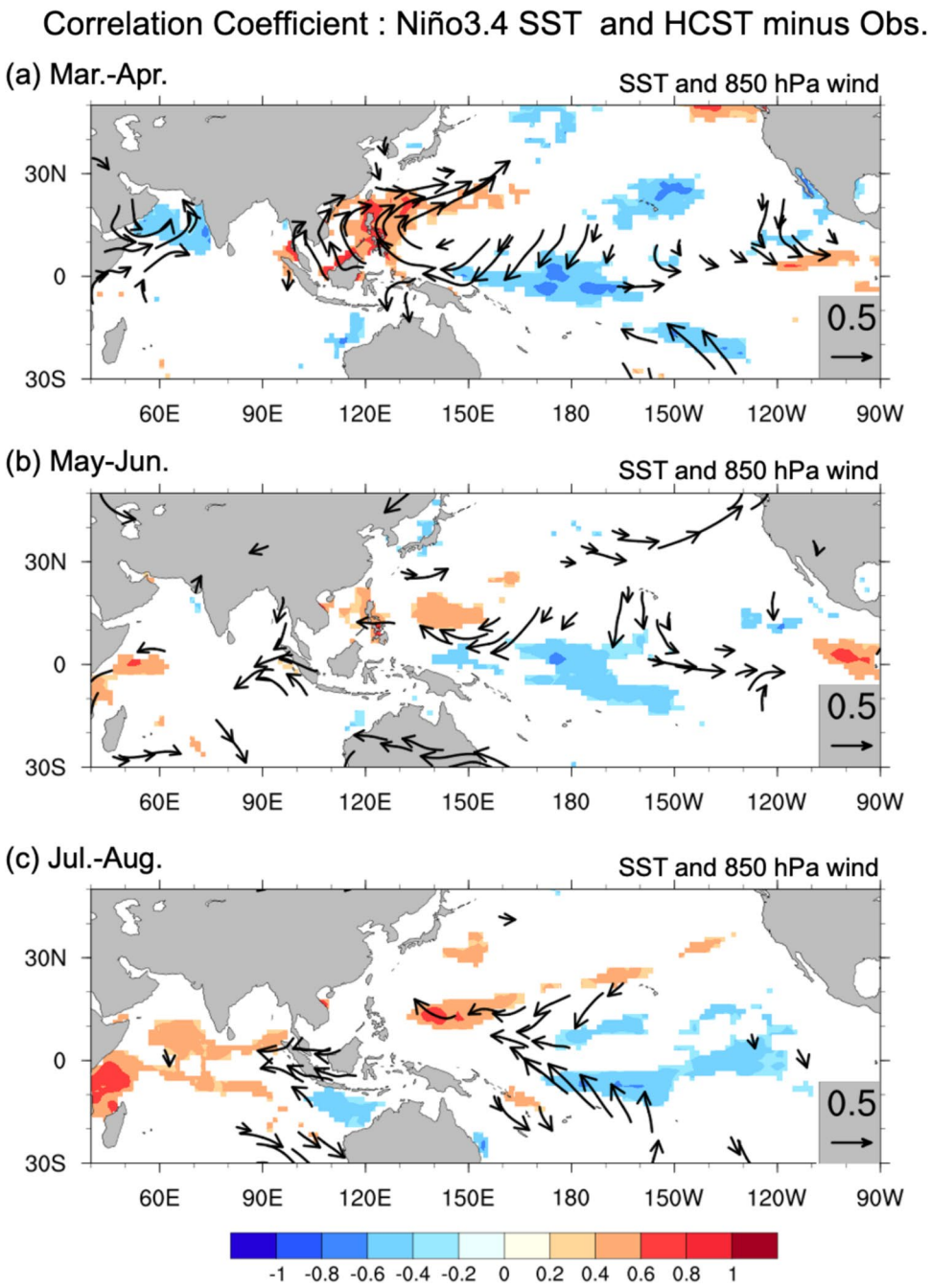


Fig. 6 Correlation coefficient maps of Niño3.4 SST index during the DJF season for the difference between the HCST and the observations in the decaying period. Shadings indicate the coefficient with SST, and vectors indicate the coefficient with 850 hPa wind. (**a**) The mean of March and April, (**b**) May and June, (**c**) July and August. Only the areas where the correlation coefficients satisfy the 95% confidence level are shown. For wind, the coefficients for U and V directions are calculated separately and displayed as a combined vector

primary cause of the errors in the 2016 HCST. This suggests a persistent potential for errors in the seasonal forecasting of the AAC associated with El Niño events in GloSea6, with the possibility of significant prediction errors during extreme events due to slight differences in the longitudinal positioning of the equatorial Pacific SST. Moreover, as it is expected that strong El Niño events will occur more frequently in the warmer world than in the present climate (Cai et al. 2014), accurate model simulations for Pacific SST cores during the decaying periods are expected to become increasingly important. This perspective also suggests the importance of interbasin sensitivity during the decaying El Niño in climate models, as differences in the sensitivity can lead to inapplicable forecasts for catastrophic climate events in our world.

4 Summary and Discussion

Despite small discrepancies of spatial patterns and intensities in the anomalies, GloSea6 HCST shows remarkable predictability of the 1997/1998 case by simulating similar spatial distributions of anomalous SST and precipitation in

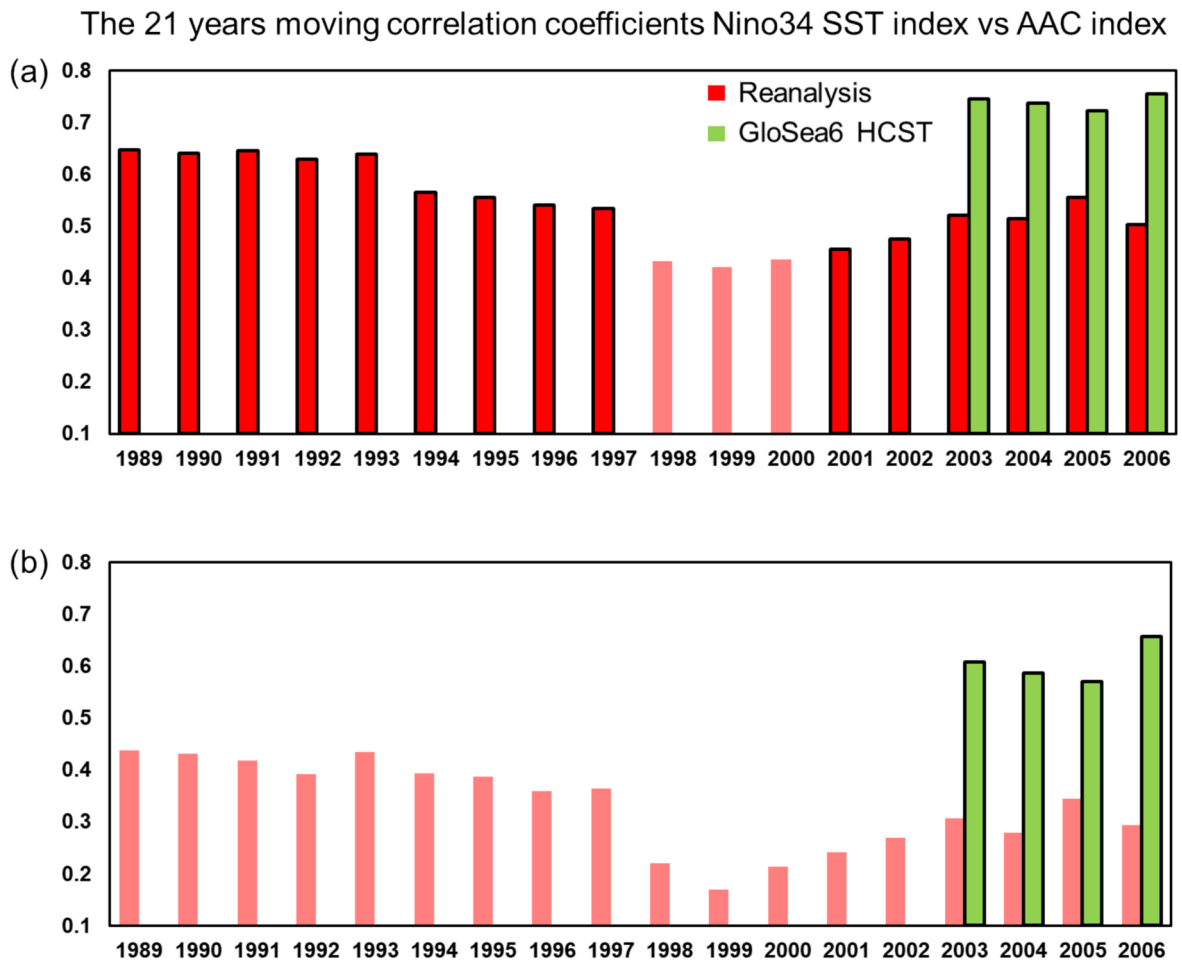


Fig. 7 (**a**) 21-year sliding correlation coefficients between the observed Niño3.4 SST (DJF season) index and the following summer (JJA) AAC of the WNP from 1979 to 2016. (**b**) same as (**a**), but with the 82/83 and 97/98 El Niño cases removed. Bars with black lines show values that are significant at the 95% confidence level, while light-colored bars indicate values that are not significant

the Indo-western Pacific region. In contrast, the 2016 HCST is quite different from the observation which shows a fast-decaying IPOC and ACC due to the fast decay of positive SST anomaly in the Indian Ocean. In the 2016 observation, a strong westerly anomaly associated with the MJO in May and this anomaly affects the summer WNP. Nevertheless, the HCST does not capture such a westerly anomaly in May and instead shows a warmer WEIO SST anomaly compared to the observations. Consequently, the persistently warmed TIO SST in the 2016 HCST results in the IPOC effect and the convective Kelvin wave continuing to influence the AAC in the WNP region through late summer. The discrepancy in 2016 is attributed to GloSea6 overestimating the regional sensitivity or relationship between the EIO and ENSO index compared to the observations. This is further demonstrated by the inaccurate simulation of the impacts of other ENSO events, not just in 2016.

Further analysis indicates that during the decaying El Niño phase in spring, GloSea6 HCST tends to simulate a colder (warmer) central (eastern) Pacific SST anomaly, which contributes to the forming the spring AAC (Jiang et al. 2019; Fan et al. 2023). This leads to the sustained warming of the WEIO SST due to the westward-propagating subsurface downwelling Rossby wave from the EEIO, more frequently than in the observations. This discrepancy contributes to sustained differences between the observations and the HCST that persist into the following summer. The observations reveal long-lasting significant correlations in the EEIO region during the decaying El Niño period, whereas correlations in the WEIO rapidly decrease in the spring. This negative IOD-like pattern generates a significant surface westerly anomaly over the TIO region in late spring season, and also impacts the Asian summer monsoon through a meridional pattern. However, the spring WEIO of the HCST responds strongly to El Niño signal, almost as much as the EEIO. As a result, the westerly anomaly does not appear as significantly as in the observations, and the cooling process in the summer

Indian Ocean is also suppressed. This represents a common error exhibited in GloSea6 during the decaying phase of El Niño, with the discrepancy in 2016 considered as one such instance.

The present study provides several points for further discussion. The gap between the model and the observations exceeds the range of 28 ensembles at 95% confidence (Fig. 2 and Fig. 3e, f). This indicates that even if signals like the MJO appear in some ensembles, they do not show the same seasonal variation as the observations. Meanwhile, we recognize that the discrepancies with the observations could be due to a larger internal variability not captured within the 28 ensembles. If the initial conditions of the HCST experiment do not exactly reflect observations, it is possible that GloSea6 HCST fails to capture some patterns or scales of internal variability. Therefore, the more accurate initial conditions could be a solution to reduce discrepancies with the observations.

Lastly, the occurrence of the IPOC during the summer is considered to play a significant role in the linear correlation between El Niño and the summer AAC (Fig. S3). The exaggerated linear relationship between El Niño and the IPOC leads GloSea6 to simulate a significant correlation with the summer AAC that does not exist in the observations. However, unlike the HCST, the observations rarely show the continuation of the IPOC into the summer following an El Niño event. This suggests that, in the HCST, a sequential and robust interbasin and interseasonal teleconnection within ENSO-TIO-AAC is simulated, whereas the observations indicate an independent relationship in which the teleconnection between ENSO and the AAC depends on the phase of the TIO. Consequently, in cases where the TIO warming does not occur during the decaying period, this may significantly impact the ability of GloSea6 to predict the influence of El Niño. Other researchers have argued that the inherent development and propagation irregularities of the MJO contribute to prediction errors in the WNP (Lu et al 2018; Shao et al. 2018; Wang et al. 2020b), highlighting the importance of processes unrelated to ENSO. For these, this study suggests that these internal variabilities interact with each other, and thus, the simulation of an exaggerated El Niño influence in GloSea6 may obscure the role of other processes.

Supplementary Information The online version contains supplementary material available at https://doi.org/10.1007/s13143-024-00388-y.

Acknowledgements This work was funded by the Korean Meteorological Administration Research and Development Program "Operation and Development of Global Seasonal Forecast System" under Grant KMA2018-00322.

Author Contributions SH and YK: conceptualization. SHH: methodology, data curation, and writing—original draft. All authors have discussed the results and contributed to writing the manuscript.

Funding KMA, 2018-00322, Yu-Kyung Hyun

Data Availability We used the atmospheric data in Global Seasonal Forecasting System version 6 (GloSea6) hindcast data. The SST, 850 hPa wind, and precipitation datasets of GloSea6 hindcast, which were interpolated in the low resolution of $2.5^{\circ} \times 2.5^{\circ}$, are available at the UKMO (United Kingdom Met Office) Sub-seasonal to Seasonal Prediction Project (S2S) re-forecast data repository, https://apps.ecmwf.int/datasets/data/s2s-reforecasts-instantaneous-accum-egrr/levtype=sfc/type=cf. The SST, 850 hPa wind, and precipitation datasets of ERA5 are available at https://www.ecmwf.int/en/forecasts/dataset/ecmwf-reanalysis-v5, and precipitation datasets in GPCP are available at https://www.ncei.noaa.gov/data/global-precipitation-climatology-project-gpcp-monthly/access/

Declarations

Conflict of Interest The authors declare that they have no conflict of interest.

Open Access This article is licensed under a Creative Commons Attribution 4.0 International License, which permits use, sharing, adaptation, distribution and reproduction in any medium or format, as long as you give appropriate credit to the original author(s) and the source, provide a link to the Creative Commons licence, and indicate if changes were made. The images or other third party material in this article are included in the article's Creative Commons licence, unless indicated otherwise in a credit line to the material. If material is not included in the article's Creative Commons licence and your intended use is not permitted by statutory regulation or exceeds the permitted use, you will need to obtain permission directly from the copyright holder. To view a copy of this licence, visit http://creativecommons.org/licenses/by/4.0/.

References

Adler, R.F., Sapiano, M.R., Huffman, G.J., Wang, J.J., Gu, G., Bolvin, D., Chiu, L., Schneider, U., Becker, A., Nelkin, E., Xie, P., Ferraro, R., Shin, D.B.: The Global Precipitation Climatology Project (GPCP) monthly analysis (new version 2.3) and a review of 2017 global precipitation. Atmosphere. **9**(4), 138 (2018). https://doi.org/10.3390/atmos9040138

An, S.-I.: A dynamic link between the basin-scale and zonal modes in the tropical Indian Ocean. Theor. Appl. Climatol. **78**, 203–215 (2004)

An, S.-I., Jin, F.F.: Nonlinearity and asymmetry of ENSO. J. Clim. **17**(12), 2399–2412 (2004)

Cai, W., Borlace, S., Lengaigne, M., Van Rensch, P., Collins, M., Vecchi, G., Timmermann, A., Santoso, A., McPhaden, M.J., Wu, L., England, M.H., Wang, G., Guilyardi, E., Jin, F.F.: Increasing frequency of extreme El Niño events due to greenhouse warming. Nat. Clim. Chang. **4**(2), 111–116 (2014)

Capotondi, A., Wittenberg, A., Newman, M., Di Lorenzo, E., Yu, J.Y., Braconnot, P., Cole, J., Dewitte, B., Giese, B., Guilyardi, E., Jin, F.F.: Understanding ENSO diversity. Bull. Am. Meteor. Soc. **96**(6), 921–938 (2015)

Chen, J., Wang, X., Zhou, W., Wang, C., Xie, Q., Li, G., Chen, S.: Unusual rainfall in southern China in decaying August during extreme El Niño 202015/2016: Role of the western Indian Ocean and north tropical Atlantic SST. J. Clim. **31**(17), 7019–7034 (2018)

Chiang, J.-C., Sobel, A.H.: Tropical tropospheric temperature variations caused by ENSO and their influence on the remote tropical climate. J. Clim. **15**(18), 2616–2631 (2002)

Du, Y., Xie, S.-P., Huang, G., Hu, K.: Role of air–sea interaction in the long persistence of El Niño–induced north Indian Ocean warming. J. Clim. **22**(8), 2023–2038 (2009)

Fan, H., Yang, S., Wang, C., Lin, S.: Revisiting Impacts of Tropical Pacific SST Anomalies on Pacific Meridional Mode during the Decay of Strong Eastern Pacific El Niño Events. J. Climate **36**, 4987 (2023). https://doi.org/10.1175/jcli-d-22-0342.1

Hersbach, H., Bell, B., Berrisford, P., Hirahara, S., Horányi, A., Muñoz-Sabater, J., Nicolas, J., Peubey, C., Radu, R., Schepers, D., Simmons, A., Soci, C., Abdalla, S., Abellan, X., Balsamo, G., Bechtold, P., Biavati, G., Bidlot, J., Bonavita, M., Chiara, G.D., Dahlgren, P., Dee, D., Diamantakis, M., Dragani, R., Flemming, J., Forbes, R., Fuentes, M., Geer, A., Haimberger, L., Healy, S., Hogan, R.J., Hólm, E., Janisková, M., Keeley, S., Laloyaux, P., Lopez, P., Lupu, C., Radnoti, G., Rosnay, P., Rozum, I., Vamborg, F., Villaume, S., Thépaut, J.N.: The ERA5 global reanalysis. Q. J. r. Meteorol. Soc. **146**(730), 1999–2049 (2020)

Hyun, S.-H., Yeh, S.-W.: Characteristics of internal variability on summer rainfall in Northeast Asia in a changing climate. Clim. Dyn. **54**(1), 1179–1195 (2020)

Jiang, F., Zhang, W., Geng, X., Stuecker, M.F., Liu, C.: Impacts of central Pacific El Niño on southern China spring precipitation controlled by its longitudinal position. J. Climate **32**, 7823–7836 (2019). https://doi.org/10.1175/JCLI-D-19-0266.1

Jin, F.F., An, S.-I., Timmermann, A., Zhao, J.: Strong El Niño events and nonlinear dynamical heating. Geophys. Res. Lett. **30**(3), 20–21 (2003)

Klein, S.A., Soden, B.J., Lau, N.-C.: Remote sea surface temperature variations during ENSO: evidence for a tropical atmospheric bridge. J. Clim. **12**, 917–932 (1999). https://doi.org/10.1175/1520-0442(1999)012/3c0917:rsstvd/3e2.0.co;2

Lau, K.-M., Weng, H.: Coherent modes of global SST and summer rainfall over China: An assessment of the regional impacts of the 1997–98 El Niño. J. Clim. **14**(6), 1294–1308 (2001)

Lee, E.-J., Jhun, J.-G., Park, C.-K.: Remote connection of the northeast Asian summer rainfall variation revealed by a newly defined monsoon index. J. Clim. **18**(21), 4381–4393 (2005)

Li, C., Chen, W., Hong, X., Lu, R.: Why was the strengthening of rainfall in summer over the Yangtze River valley in 2016 less pronounced than that in 1998 under similar preceding El Niño events?—Role of midlatitude circulation in August. Adv. Atmos. Sci. **34**, 1290–1300 (2017)

LinHo, W.B.: The time–space structure of the Asian-Pacific summer monsoon: a fast annual cycle view. J. Clim. **15**(15), 2001–2019 (2002)

Lu, B., Ren, H.-L., Scaife, A.A., Wu, J., Dunstone, N., Smith, D., Wan, J., Eade, R., MacLachlan, G.M.: An extreme negative Indian Ocean Dipole event in 2016: dynamics and predictability. Clim. Dyn. **51**, 89–100 (2018)

MacLachlan, C., Arribas, A., Peterson, K.A., Maidens, A., Fereday, D., Scaife, A.A., Gordon, M., Vellinga, M., Williams, A., Comer, R.E., Camp, J., Xavier, P., Madec, G.: Global Seasonal forecast system version 5 (GloSea5): A high-resolution seasonal forecast system. Q. J. r. Meteorol. Soc. **141**(689), 1072–1084 (2015)

Murakami, T., Matsumoto, J.: Summer monsoon over the Asian continent and western North Pacific. J. Meteorol. Soc. Japan Ser. II **72**(5), 719–745 (1994)

Santoso, A., Mcphaden, M.J., Cai, W.: The defining characteristics of ENSO extremes and the strong 2015/2016 El Niño. Rev. Geophys. **55**(4), 1079–1129 (2017)

Shao, X., Li, S., Liu, N., Song, J.: The Madden-Julian oscillation during the 2016 summer and its possible impact on rainfall in China. Int. J. Climatol. **38**(5), 2575–2589 (2018)

Wang, B., Wu, R.-G., Fu, X.-H.: Pacific-east Asian teleconnection: How does ENSO affect east Asian climate? J. Climate **13**, 1517–1536 (2000). https://doi.org/10.1175/1520-0442(2000)013%3c1517:PEATHD%3e2.0.CO;2

Wang, B., Wu, R.-G., Li, T.: Atmosphere-warm ocean interaction and its impacts on Asian-Australian monsoon variation. J. Clim. **16**, 1195–1211 (2003). https://doi.org/10.1175/1520-0442(2003)16/3c1195:aoiaii/3e2.0.co;2

Wang, B., Li, J., He, Q.: Variable and robust East Asian monsoon rainfall response to El Niño over the past 60 years (1957–2016). Adv. Atmos. Sci. **34**(10), 1235–1248 (2017)

Wang, C.-Y., Xie, S.-P., Kosaka, Y.: ENSO-unrelated variability in Indo-Northwest Pacific climate: Regional coupled Ocean-Atmospheric feedback. J. Clim. **33**(10), 4095–4108 (2020a)

Wang, X., Xie, S.-P., Guan, Z.: Atmospheric internal variability in the summer Indo-Northwestern Pacific: Role of the intraseasonal oscillation. J. Clim. **33**(8), 3395–3410 (2020b)

Wen, N., Liu, Z., Liu, Y.: Direct impact of El Niño on East Asian summer precipitation in the observation. Clim. Dyn. **44**, 2979–2987 (2015)

Xie, S.-P., Annamalai, H., Schott, F.A., McCreary, J.P.: Structure and mechanisms of South Indian Ocean climate variability. J. Clim. **15**(8), 864–878 (2002)

Xie, S.-P., Hu, K., Hafner, J., Tokinaga, H., Du, Y., Huang, G., Sampe, T.: Indian Ocean capacitor effect on Indo–western Pacific climate during the summer following El Niño. J. Clim. **22**(3), 730–747 (2009)

Xie, S.-P., Kosaka, Y., Du, Y., Hu, K., Chowdary, J.S., Huang, G.: Indo-western Pacific Ocean capacitor and coherent climate anomalies in post-ENSO summer: A review. Adv. Atmos. Sci. **33**(4), 411–432 (2016)

Yoon, J., Yeh, S.-W.: Influence of the Pacific decadal oscillation on the relationship between El Niño and the northeast Asian summer monsoon. J. Clim. **23**(17), 4525–4537 (2010)

Zhang, W., Li, H., Jin, F.F., Stuecker, M.F., Turner, A.G., Klingaman, N.P.: The annual-cycle modulation of meridional asymmetry in ENSO's atmospheric response and its dependence on ENSO zonal structure. J. Climate **28**, 5795–5812 (2015). https://doi.org/10.1175/JCLI-D-14-00724.1

Zhang, P., Xie, S.-P., Kosaka, Y., Lutsko, N.J., Okumura, Y.M., Miyamoto, A.: Why East Asian monsoon anomalies are more robust in post El Niño than in post La Niña summers. Nat. Commun. **15**(1), 7401 (2024)

Publisher's Note Springer Nature remains neutral with regard to jurisdictional claims in published maps and institutional affiliations.